



Positron annihilation lifetime measurement and X-ray analysis on 120 MeV Au⁺⁷ irradiated polycrystalline tungsten



Charu Lata Dube^{a,*}, Pawan Kumar Kulriya^b, Dhanadeep Dutta^c, Pradeep K. Pujari^c, Yashashri Patil^a, Mayur Mehta^a, Priyanka Patel^a, Samir S. Khirwadkar^a

^a Divertors & First-Wall Technology Development Division, Institute for Plasma Research, Gandhinagar, 382428, India

^b Materials Science Group, Inter University Accelerator Centre, New Delhi, 110016, India

^c Radiochemistry Division, Bhabha Atomic Research Centre, Mumbai, 400 085, India

H I G H L I G H T S

- Simulation of neutron damage in W using 120 MeV Au⁺⁷ ion irradiation has been employed.
- The induction of damages is attributed to high electronic energy losses.
- Positron annihilation lifetime measurements confirm induction of bulk damages.
- The physical properties of damaged tungsten have been investigated.

A R T I C L E I N F O

Article history:

Received 17 February 2015

Received in revised form

14 May 2015

Accepted 15 May 2015

Available online 3 June 2015

Keywords:

Heavy ion irradiation

Positron annihilation spectroscopy

X-ray diffraction

Polycrystalline tungsten

Radiation damage

A B S T R A C T

In order to simulate radiation damages in tungsten, potential plasma facing materials in future fusion reactors, surrogate approach of heavy ion irradiation on polycrystalline tungsten is employed. Tungsten specimen is irradiated with gold heavy ions of energy 120 MeV at different fluences. Positron annihilation lifetime measurements are carried out on pristine and ion beam irradiated tungsten specimens. The variation in positron annihilation lifetime in ion irradiated specimens confirms evolution of vacancy clusters under heavy ion irradiation. The pristine and irradiated tungsten specimens have also been characterized for their microstructural, structural, electrical, thermal, and mechanical properties. X-ray diffractograms of irradiated tungsten specimens show structural integrity of polycrystalline tungsten even after irradiation. Nevertheless, the increase in microstrain, electrical resistivity and microhardness on irradiation indicates creation of lattice damages inside polycrystalline tungsten specimen. On the other hand, the thermal diffusivity has not change much on heavy ion irradiation. The induction of damages in metallic tungsten is mainly attributed to high electronic energy loss, which is 40 keV/nm in present case as obtained from SRIM program. Although, concomitant effect of nuclear losses on damage creation cannot be ignored. It is believed that the energy received by the electronic system is being transferred to the atomic system by electron-phonon coupling. Eventually, elastic nuclear collisions and the transfer of energy from electronic to atomic system via inelastic collision is leading to significant defect generation in tungsten lattice.

© 2015 Elsevier B.V. All rights reserved.

1. Introduction

In future fusion reactors, a large number of high energy (14.1 MeV) neutrons will be generated by deuterium–tritium

fusion reactions. These neutrons will irradiate the reactor wall and in turn the physical properties of reactor wall material will get modified [1,2]. Tungsten is considered as the most likely material to be used in divertor section of ITER-like Tokamak, because of its attractive physical properties e.g. it can withstand high temperatures, low activation, does not transmute into long-lived radioactive isotopes and has a low erosion rate [3]. All these properties make tungsten prime material for fabricating plasma facing components for fusion applications. However, in fusion reactor, the high

* Corresponding author. Immobilisation Science Laboratory, Department of Materials Science and Engineering, University of Sheffield, Sheffield, S1 3JD, England.
E-mail addresses: dubecharu@gmail.com, c.l.dube@sheffield.ac.uk (C.L. Dube).

flux of energetic neutrons (14.1 MeV) will create a large number of radiation damages in tungsten and it will lead to change in thermo-mechanical properties of tungsten [4,5].

Interaction of neutron with plasma facing material induces both elastic and inelastic nuclear reactions. Inelastic interaction of neutrons with solid activates transmutation process inside solid. During elastic interaction, an incident neutron transfers energy to a lattice atom, forming a primary knock-on atom (PKA). PKA dislodges neighbouring atoms, which results in an atomic displacement cascade and formation of point defects and defect clusters of vacancies and interstitial atoms inside the solid. The induction of damages modifies thermo-mechanical properties of tungsten and, thus, it is imperative to understand the effect of radiation induced damage, on thermo-mechanical properties of tungsten.

Neutron source of energy 14.1 MeV and required fluence is not yet available and existing neutron irradiation facilities are being used. Specimens irradiated with neutrons get radioactive in nature and needs dedicated laboratory set up to investigate the radiation modified physical properties [6], and it limits the number and types of test that can be performed on neutron irradiated specimens. Alternatively, high energy (nearly 1 MeV/amu) heavy ion beams can be employed to simulate similar kind of radiation damages inside plasma facing materials; so that damage induced modification in their properties can be studied [7].

During ion solid interactions, at low incident ion energy (up to 100 keV), ions transfer their energy mainly via elastic nuclear stopping (S_n), which leads to damage creation in solids. The damage creation in tungsten due to nuclear stopping is limited to top few nanometres only due to high density (19.3 g/cm^3) of tungsten. At high energies, ions can penetrate up to few micron deep in bulk and can lead to bulk damage creation via elastic and inelastic collisions [8,9].

However, neutron-solid and ion–solid interactions are different in nature. Since ions are electrically charged, their penetration inside solid is limited and depends on incident ion energy and mass. On the other hand, neutron (electrically neutral in nature) penetrates deep inside the solid and results in bulk damages. Oya et al. have reported different thermal desorption spectra for neutron and ion irradiated W specimens [10]. The additional desorption stage for neutron irradiated W specimen, had been attributed to deeper deuterium trapping in irradiated W specimens owing to bulk damages. In case ion irradiated W specimens, damages are limited to a depth of less than $1 \mu\text{m}$ and hence shallow trapping of deuterium, which gets reflected in desorption spectra [10]. Furthermore, neutron participates in nuclear activity, while ion–solid interaction is electrostatic in nature. Nevertheless, the damage creation due to elastic interaction of neutrons with solid is nearly similar to damage creation by ions via elastic and inelastic interactions, therefore, ions are being widely employed to simulate radiation damage inside solids.

World wide efforts are being made to correlate heavy ion induced damages to neutron induced damages. Kirk et al. [11] attempted to simulate neutron induced damages by employing Kr ions irradiation in Mo and further research is in progress to establish correlation between two methods. Armstrong et al. used 2 MeV tungsten ion beam to simulate neutron damage in tungsten alloy, subsequently, damage induced change in mechanical properties had been investigated [5,12]. Takagi et al. employed 1.5 and 5 MeV self-ion irradiation on tungsten to study deuterium trapping in damaged tungsten [13]. Shimada et al. have performed series of extensive studies on fuel retention, their depth profiling and fuel desorption in damaged tungsten [14–16]. Hatano et al. have also carried out deuterium retention studies on the neutron and ion irradiated tungsten specimens [17]. Khripunov et al. utilized high energy light ions helium and carbon, to produce displacement

damage in tungsten [18]. Recently, Ogorodnikova et al. have used 20 MeV self-ion irradiation in tungsten to perform study on accumulation and recovery of radiation defects in tungsten [19]. They have also performed TEM and fuel retention study in self-ion damaged W [20,21].

At high energies, incident energetic ions deposit their energy in electronic system of target atoms and the deposited energy gets transferred to atomic system of target atoms through electron–electron and electron-phonon coupling. The electron-phonon coupling strength plays important role in defect generation in solids. Metals such as Ti and Fe exhibit strong electron-phonon coupling and electronic stopping lead to defect creation in these materials. Increase in defect-production efficiency in metal system e.g. Bi, Ti, and Fe is well evidenced [22]. The electron-phonon coupling strength of materials defined as $g = D_e C_e / \lambda^2$ (D_e : electronic diffusivity, C_e : electronic specific heat and λ is electron mean free path), depends on electronic parameters [23]. Daraszewicz et al. have estimated the effective electron-phonon coupling constant (g) for tungsten from *ab initio* calculations and high-resolution pump-probe reflectivity measurements and it is found to be $1.4 \times 10^{17} \text{ Wm}^{-3} \text{ K}^{-1}$ [24]. The significant value of g indicates efficient energy transfer from electronic to atomic system in case of tungsten.

It has been reported that, in conductors, the energy stored into the electronic excitation can affect materials properties depending upon the value of electronic stopping power (S_e) of the ion. If S_e value, which depends on the material, exceeds a certain threshold ($\sim 10\text{--}40 \text{ keV/nm}$) then electronic stopping can also contribute to additional disorders in the material i.e. atomic displacements can occur due to electronic energy losses as well under certain conditions e.g. in case of Ti metal [25], the S_e threshold for defect creation is reported to be $11\text{--}14 \text{ keV/nm}$ [26,27]. Electronic stopping power (S_e) of 120 MeV gold ions in tungsten is evaluated from SRIM/TRIM simulation software [28]. The obtained energy loss spectrum of gold ions in tungsten is shown in Fig. 1, and it shows electronic energy loss of $\sim 40 \text{ keV/nm}$ for 120 MeV gold ions. Therefore, in the present work, 120 MeV gold ions have been chosen to get high value of $S_e \sim 40 \text{ keV/nm}$, so that electronic stopping can contribute significantly in bulk damage creation in tungsten. At the same time gold and tungsten have nearly similar atomic mass/size and no known phases of gold and tungsten exist, therefore, gold implantation in tungsten will not give any modification in properties due

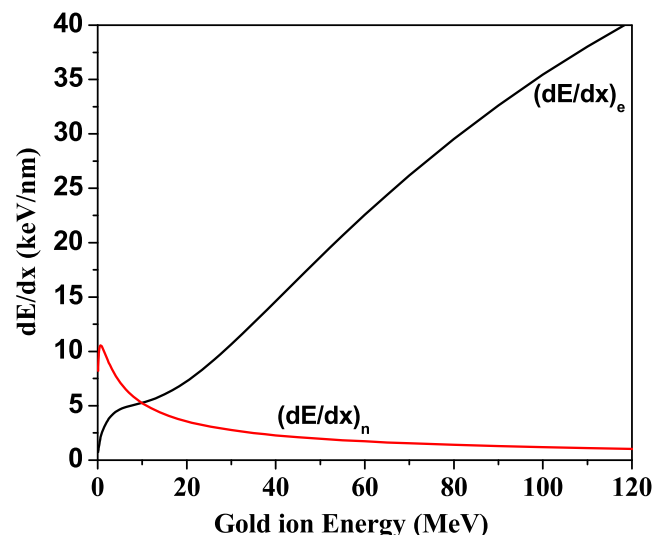


Fig. 1. Energy loss spectra of gold ions in tungsten obtained from SRIM software.

to chemical changes. By the employed approach, bulk damages in W can be produced and hence estimation of physical properties of irradiated tungsten will get easier.

2. Experimental details

Tungsten specimens of size 8*8*3 mm were cut from Tungsten sheet (procured from Plansee Ltd. as hot rolled sheet) and were polished. Prior to irradiation experiment, the particle size measurement was performed as per ASTM standard E112 and it revealed that polycrystalline tungsten has average particle size (APS) of six micron. The specimens, taken from W sheet and polished, are refereed as pristine W (PW). One set of PW specimens had been annealed at ~1173 K under ultra-high vacuum conditions for one hour. Heavy ion irradiation had been performed on pristine W (PW) and annealed W (AW) specimens. In order to induce radiation damage inside tungsten, gold ion beam from the 15 UD Pelletron at Inter University Accelerator Centre, Delhi, had been used for irradiating polycrystalline tungsten specimens. Tungsten specimens of dimensions of 8*8*3 mm, were irradiated with gold ions of energy 120 MeV at different fluences given in Table 1. The gold ion beam was rastered over the specimen to generate different doses at beam current of 0.5 pA and as the beam current was very low, no increase in the specimen temperature was expected. The damage profile in tungsten irradiated at different fluence with gold ions is shown in Fig. 2. It can be seen that the maximum damage depth is 7 micron, with a peak at 5 micron. The damage levels are estimated from TRIM calculations with full cascade option and displacement energy is taken as 90 eV [12].

For direct evidence of defect generation inside tungsten, positron annihilation lifetime measurements were carried out using two plastic scintillation detectors coupled to fast–fast coincidence system with a timing resolution of 260 ps. The ^{22}Na isotope (~10 μCi) wrapped in a Kapton foil was used as the positron source. The positron source was sandwiched between two identical pieces of the tungsten specimens. The sandwich of tungsten specimen – positron source–tungsten specimen, was kept between two detectors. A total number of 10^6 data points were collected for each spectrum. The data analysis was done using PATFIT program [29].

The microstructural, structural, electrical, thermal and mechanical properties were investigated before and after irradiation, to probe the effect of ion induced damages on various properties of tungsten. The microstructural analysis was carried on JEOL (JSM7600F) FESEM system. The X-ray diffractograms (XRD) of the specimens before and after irradiation were recorded by using D-8 X-ray diffractometer (Bruker AXS Germany) in θ – 2θ geometry by using Cu $K_{\alpha 1}$ X-rays. The electrical resistivity of pristine and irradiated specimen was measured using linear four probe method by using Keithley source (Model no. 2400) and nanovoltmeter (Model no. 2182). The thermal diffusivity of specimen was obtained using laser flash method on Flashline 5000 thermal properties analyser system. The mechanical property of pristine and irradiated

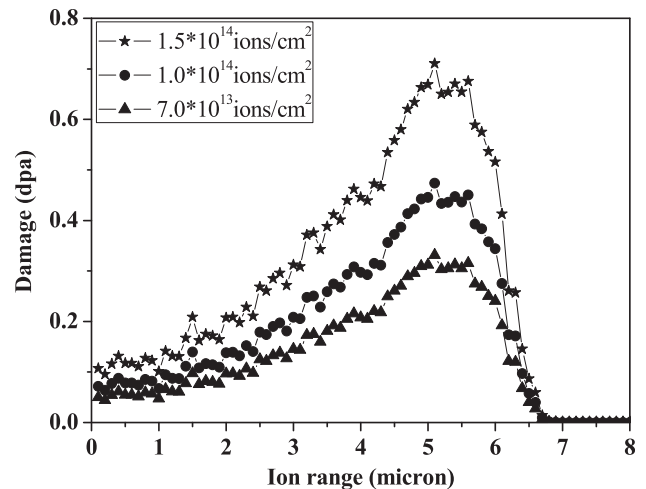


Fig. 2. TRIM calculation showing the damage profile in tungsten irradiated with Au ions of energy 120 MeV.

tungsten specimens was investigated by employing Micro Vicker's hardness tester (Mitutoyo HM211). The applied load was 10 g and the time of indentation was kept constant at 10 s for all measurements.

3. Results and discussion

Positron, the anti-particle of an electron, after being implanted into a solid sample gets thermalized very fast (within few ps) through the interaction with the surrounding medium and may get trapped into a defect before annihilating with an electron. The lifetime of trapped positron inside defect is inversely proportional to the electron density seen by the positron. The reduced electron density at the vacant/defect site increases the positron lifetime, and positron lifetime increases as the size of defect increases. It is reported that the positron lifetime in a defect-free single crystal of tungsten is $\tau_f \sim 0.105$ ns and in general, the estimated positron lifetime in mono and di vacancies in tungsten are $\tau_{1v} = 1.3\tau_f$ (~0.136 ns) and $\tau_{2v} = 1.5\tau_f$ (~0.157 ns) [30]. However, different groups have reported positron lifetime in tungsten mono-vacancy (or in dislocation loop) in the range of 0.16–0.20 ns [31]. The theoretically calculated di-vacancy lifetime is reported to be 0.23 ns and it is 0.41 ns–0.44 ns for nano-voids having 13–37 vacancies in tungsten [32]. In the present investigation, mainly two positron lifetime components τ_1 (0.13–0.18 ns) and τ_2 (~0.28–0.38 ns) along with their respective intensities I_1 and I_2 are observed in the PW, AW, and ion irradiated tungsten specimens. A third component τ_3 (~1.9 ns) with very less intensity (~4%) was also observed in AW and all irradiated specimens. Here, τ_1 is in the range of positron lifetime trapped in mono vacancy-like defects; also a fractional contribution from di-vacancy like defects is possible to be included in τ_1 in the

Table 1
Specimen classification, Fluence, and XRD structural parameters for pristine and irradiated tungsten specimen.

Specimen name	Specimen state	Fluence (ions/cm ²)	XRD peak position (2 θ) in degree for (110) peak	FWHM of (110) XRD peak	Lattice strain ($\times 10^{-3}$)	Grain size (nm)
Pristine W (PW)	As received	–	40.28	0.2368	2.19 ± 0.07	164
PW:1e14	Do	1×10^{14}	40.24	0.2360	2.20 ± 0.31	159
PW:1.5e14	Do	1.5×10^{14}	40.25	0.2208	2.10 ± 0.12	200
Annealed W (AW)	Annealed Tungsten	0	40.25	0.2400	–	–
AW:7e13	Do	7×10^{13}	40.27	0.2432	2.20 ± 0.31	180
AW:1.5e14	Do	1.5×10^{14}	40.25	0.2560	1.96 ± 0.19	96

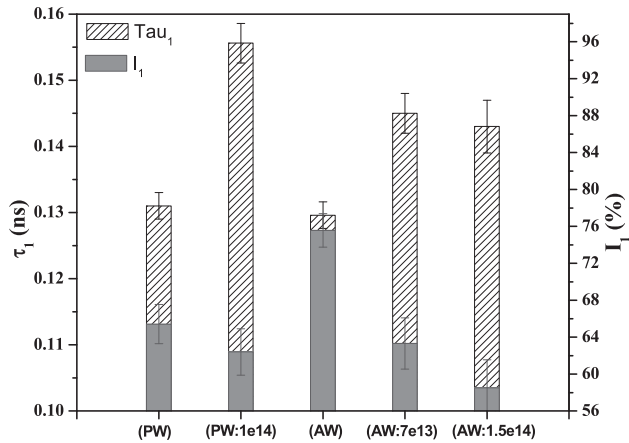


Fig. 3. Variation of τ_1 and corresponding intensity (I_1) for tungsten specimens.

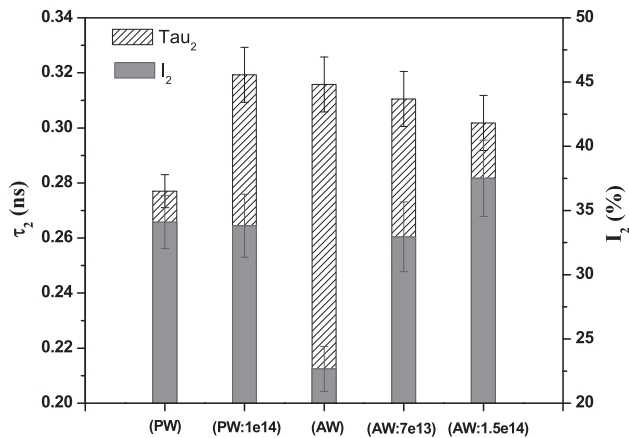


Fig. 4. Variation of τ_2 and corresponding intensity (I_2) for tungsten specimens.

irradiated samples. The second component τ_2 is the convolution of positron lifetime trapped in di vacancies and the nano-voids/vacancy cluster having different number of vacancies. The third component (τ_3) represents the ortho-positronium lifetime in larger voids.

The variation of τ_1 and τ_2 components of positron life time and corresponding intensities (I_1 and I_2) are shown in Figs. 3 and 4. The values of positron lifetime components τ_1 and τ_2 for pristine W (PW) shows that PW specimen is not defect-free as in case of defect-free crystal of tungsten positron lifetime should be ~ 0.105 ns. In both the PW and AW (annealed W) specimens, the τ_1 has almost same value (~ 0.13 ns), which arises from the pure mono vacancy like defects. Furthermore, in the case of AW specimen, it is interesting to note that intensity (I_1) is high as compared to that of PW. It indicates that AW has more “pure mono vacancy” like defects. In addition, the positron lifetime (τ_2) for AW specimen is higher as compared to that of PW but at the same time substantial reduction in intensity (I_2) from $\sim 34\%$ to $\sim 22\%$ is observed. From the obtained results, two conclusions can be drawn: (i) possible dissociation of small vacancy–impurity complexes if any, which generally occurs at ~ 573 K as pointed out by Debelle et al. [33], and this phenomenon can lead to an increase in the concentration of mono-vacancies; (ii) probable migration of self-interstitials (which requires only 0.054 eV [34] activation energy) can result into conversion of di-vacancies/vacancy clusters into mono-vacancies. Therefore, increase in mono vacancy concentration is very much

expected and is evidenced as well. Debelle et al. have mentioned that larger vacancy like clusters can migrate during stage II annealing (from 773 K to 1723 K), therefore, void formation in AW specimen can be attributed to migration of larger vacancy like clusters.

In case of irradiated PW (IPW) namely PW:1e14, the increase in τ_1 from 0.13 to 0.15 and τ_2 from 0.27 to 0.31 ascertains formation of vacancy clusters on heavy ion irradiation. This is attributed to evolution of new vacancy clusters from damage cascades evolving during heavy ion irradiation. The τ_1 value for irradiated AW (IAW) specimens (AW:7e13 and AW:1.5e14) is more than that in AW specimen, which is a sign of evidence that AW:7e13 and AW:1.5e14 have mono as well as di-vacancies, whereas AW has more pure mono-vacancy like defects. The τ_2 components in AW:7e13 and AW:1.5e14, is nearly close to that for AW, but intensity I_2 is relatively high for irradiated annealed W specimens. The increase in I_2 suggests generation of more vacancies (in addition to existing one) during ion irradiation on AW specimens. This increase in I_2 arises at the expense of I_1 , as the intensity I_1 is seen to decrease in PW:1e14, as well as in AW:7e13 and AW:1.5e14 as compared to un-irradiated specimens. Since, the intensity I_1 represents the concentration of mono and di-vacancy like defects in the irradiated specimens, the reduction in I_1 indicates that during irradiation more and more mono and di-vacancy like defects get migrated and produce more number of vacancy clusters which is represented in increase in I_2 . In the present work, the obtained damage rate is $\sim 10^{-4}$ dpa/sec. Kinetic Monte-Carlo simulations, performed by Yamamoto et al. suggests damage rate of 10^{-4} dpa/sec is sufficient for void nucleation in tungsten during irradiation [25] and therefore the formation of void is very much probable in irradiated W specimens. The observed ortho-positronium lifetime component (τ_3) for IPW and IAW specimens indicates the presence of voids inside IPW and IAW specimens. The formation of void is attributed to irradiation induced migration of vacancy clusters. Scanning electron images have been taken (at random locations) before and after irradiation on W specimens. The voids are seen for irradiated specimen, however only for specimens irradiated at high fluence (1.5e14) due to constraints of SEM machine. The voids are clearly visible in FESEM image of PW:1.5e14 specimen, as shown in Fig. 5. The ion irradiation induced void formation is widely reported by several other groups as well [35,36].

The tungsten specimens have been characterized for their structural parameters by using X-ray diffraction (XRD) method

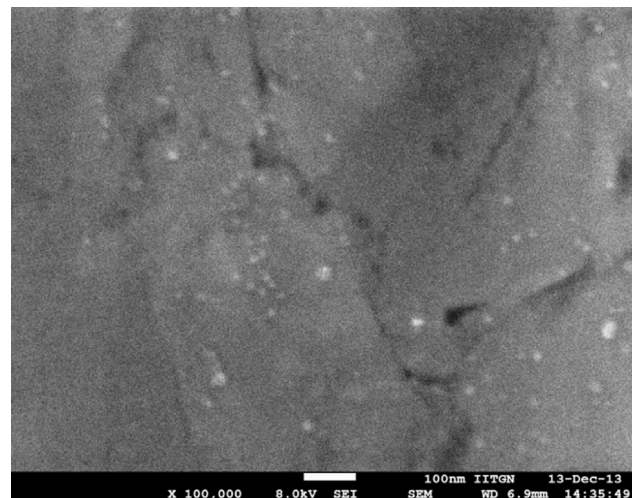


Fig. 5. FESEM image of PW:1.5e14 tungsten specimen.

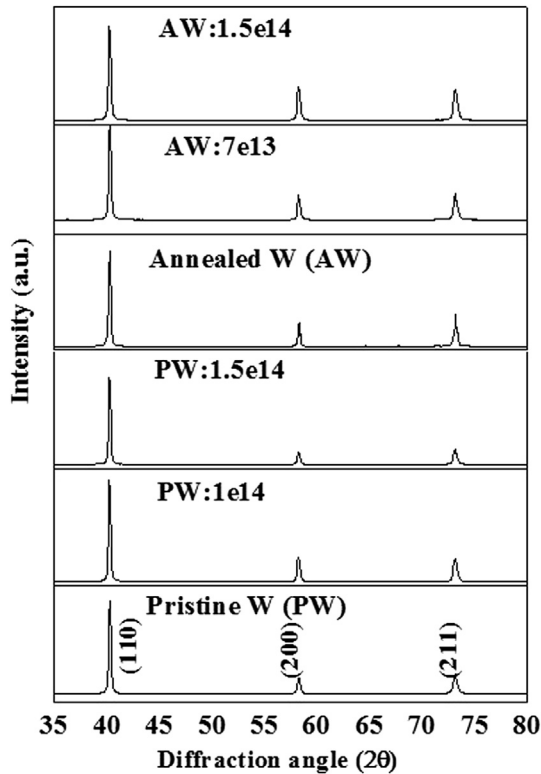


Fig. 6. X-ray diffractogram of pristine and irradiated tungsten specimens.

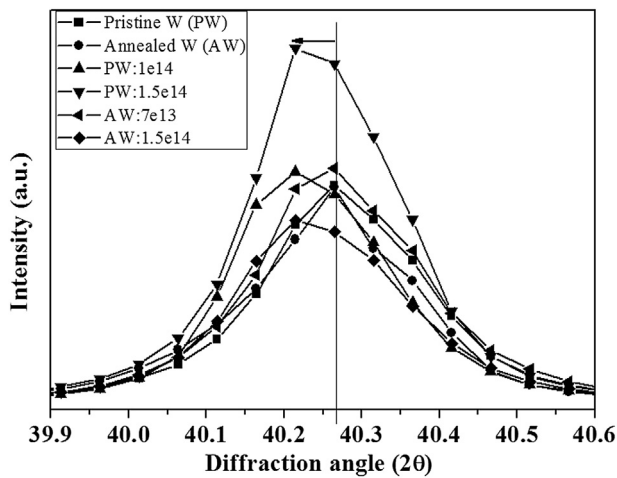


Fig. 7. Enlarged view of X-ray diffractogram of pristine and irradiated tungsten specimens.

before and after irradiation. The X-ray diffraction peaks have been fitted with pseudo-Voigt function for evaluation of peak positions (2θ), FWHM (β_{obs}) and intensity. The diffraction angle (2θ) and FWHM for (110) XRD peak are given in Table 1. The XRD patterns of W specimens before and after irradiation are shown in Figs. 6 and 7, and it is found that XRD peaks are in conformity with the bcc structure of tungsten and are in good agreement with the data of JCPDS file No.040806. There is no evidence of structural phase transformation in irradiated tungsten specimen, which indicates that integrity of crystal structure is intact even after irradiation. However, the shift has been observed in diffraction angle (2θ) for (110) XRD peak (Fig. 7) before and after ion irradiation, which suggests probable presence of micro-strain in W specimens. To

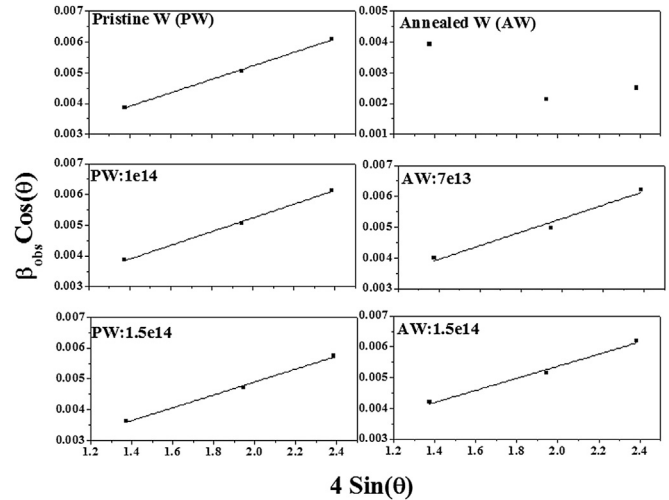


Fig. 8. Williamson Hall plot for pristine and irradiated tungsten specimen.

evaluate the nature and quantum of micro-strain, Williamson Hall method has been adopted [37]. The small grain size (<200 nm) and micro-strain both contribute to broadening of XRD peak, but differently. In order to evaluate strain (ϵ) and crystallite size (D), $\beta_{\text{obs}}\text{Cos}(\theta)$ vs $4\text{Sin}(\theta)$ graphs have been drawn for each specimens, and plots are shown in Fig. 8. Micro-strain and crystallite size are calculated from the slope and y-intercept of the fitted line, as shown in Fig. 8, respectively. The estimated values of micro-strain and grain size are given in Table 1. The XRD peak position for pristine W is observed at higher 2θ value as compared to AW specimen. It is probable that compressive strain was present in as received pristine W, which has got relaxed after annealing. Further, Williamson-Hall plot also confirms that lattice strain has got relaxed after annealing as $\beta_{\text{obs}}\text{Cos}(\theta)$ vs $4\text{Sin}(\theta)$ variation is not linear. On the other hand, in irradiated PW specimens (PW:1e14 and PW:1.5e14), the XRD peaks shift towards lower 2θ value. It can be inferred that heavy ion irradiation on as received pristine W specimen is changing nature of micro-strain from compressive to tensile in case of PW:1e14 sample. Radiation induced defects such as vacancies, interstitials etc., affects the crystal parameter by changing the (average) lattice parameter. This may cause a strain gradient which results in lattice distortions and hence change in the type of strain. The presence of tensile micro-strain in irradiated tungsten specimen can be attributed to generation of defects/dislocation loops etc. In addition, grain growth is also observed in case of PW:1.5e14 specimen. The atomic movement during grain growth can be driven by various factors such as high temperature, an intermediate temperature with a moderate external pressure (hot isostatic pressing), or a lower temperature with a high stress [38]. The observed grain growth in present case, can be attributed to localized damage caused by the energetic heavy ion irradiation in the vicinity of grain boundary, which is the likely driving force for grain growth in case of PW:1.5e14 specimen [39]. Interestingly, it appears that certain critical dose is required to get sufficient damage near grain boundary to initiate grain growth as grain growth is absent in case of PW:1e14 specimen irradiated for low fluence. Furthermore, as a consequence of grain growth there is decrease in internal lattice strain and hence decrease in FWHM of (110) peak is well understood (Table 1). Similar kind of grain growth has also been reported by Wang et al. in case of W thin films irradiated with 4 MeV Au ions [40]. Wang et al. have observed complete phase transformation from beta to alpha phase W induced by ion irradiation at high fluence. The grain growth has been observed

Table 2
Physical properties of pristine and irradiated tungsten specimen.

Specimen name	Electrical resistivity ($\times 10^{-8} \Omega \text{ m}$)	Thermal diffusivity (cm^2/sec)	Microhardness (MPa)
PW	13.5	0.6621	722 ± 17
PW:1.5e14	20.4	0.6677	777 ± 10

as per power law expression, which relates the average grain size to the ion fluence. They suggest that grain growth is not due to thermal activation; instead, defect stimulated is the dominated mechanism.

In the case of ion irradiation on AW specimens, induction of lattice strain is found, which is again attributed to generation of defects/dislocation loops etc. inside polycrystalline annealed tungsten specimens. Contrary to finding in case of ion irradiation on pristine W specimen, grain refinement is observed for AW:1.5e14, which may owe its origin in formation of nanostructure on normal ion incidence as observed in other metallic systems [41]. It is strongly believed that the presence of micro strain in W specimens prior to irradiation, is playing crucial role in micro-structure development of irradiated specimens. In presence of micro-strains, it seems that threshold for grain growth is being easily achieved and hence grain growth is occurring. While in case of ion irradiation on annealed W specimen, which is free from micro-strain (as revealed from Williamson Hall analysis), the well reported grain refinement is observed. Hence it is concluded that internal strain has major role in defining the microstructure in present case.

In addition, attempts have also been made to measure changes in irradiated tungsten's physical properties by measuring changes in electrical resistance, thermal diffusivity and microhardness. The electrical resistivity of PW and IPW is measured in linear four probe geometry, and values are given in Table 2. The current carrying wires were of tungsten, and prior to resistivity measurement it has been assured that contact is ohmic in nature. The electrical resistivity of pristine tungsten specimen (procured from Plansee Ltd. as hot-rolled sheet) is found to be $13.5 \times 10^{-8} \Omega \text{ m}$. The measured electrical resistivity of pristine tungsten specimen is close to reported electrical resistivity value ($5.9 \times 10^{-8} \Omega \text{ m}$ for pure tungsten procured from Plansee Ltd.) by Fukuda et al. [42]. They have observed increase in electrical resistivity value ($\sim 7.5 \times 10^{-8} \Omega \text{ m}$) for pure tungsten after neutron induced damage of 0.15 dpa. The neutron irradiation was performed at Japan Materials Testing Reactor (JMTR) and the increase in resistivity is attributed to displacement damage and the formation of defect clusters in neutron irradiated tungsten specimen. We have also found an increase in electrical resistivity for heavy ion irradiated tungsten specimen and measured value of electrical resistivity is $20.4 \times 10^{-8} \Omega \text{ m}$. The increase in electrical resistivity is in conformity with X-ray diffraction and positron annihilation life time results and confirms generation of defects/dislocation loops inside heavy ion irradiated tungsten specimen. The increase in electrical resistivity of IPW sample is attributed to increased scattering of electrons from irradiation induced defects during transport of electrical current. Furthermore, as suggested by Dunlop et al. that increase in resistivity is an indication that defects are being created from uncollapsed displacement cascades. Therefore, increases in resistivity for PW:1.5e14 specimen suggest that displacement cascades are not overlapping at fluence of 1.5×10^{14} ions/cm² and eventually ending in significant generation of defects inside polycrystalline tungsten [43].

The thermal diffusivity measurement results, obtained from laser flash method, are given in Table 2. The thermal diffusivity value of pristine and irradiated tungsten specimen are very close to

each other. In solids, the total thermal conductivity is sum of electronic and lattice thermal conductivity and in case of tungsten, at room temperature, electronic thermal conductivity is dominant [44]. In solids, heat is transported by entropy (spin and charge of electron) and electric current by charge alone [45]. Therefore, scattering of electrons from defects will be high during electrical current transport as compared to heat transfer and the fact is evidenced from observed changes in electrical resistivity and electronic thermal diffusivity values. After ion irradiation electrical resistivity has increased, on the other hand only marginal increase is observed for thermal diffusivity value. Furthermore, the ion beam induced damages are embedded up to 7 micron only as obtained for TRIM simulations. The thermal diffusivity measurements have been performed on 3 mm thick tungsten specimen. Therefore, the thermal diffusivity of damaged layer will not be affecting much the thermal diffusivity of 3 mm thick tungsten specimen and this can be one of the reasons for insignificant change in thermal diffusivity value after irradiation.

To investigate the effect of heavy ion irradiation on mechanical properties of tungsten, microhardness measurements are performed on pristine and ion beam irradiated tungsten specimen, the microhardness values are given in Table 2. Increase in microhardness is observed for irradiated specimen. The microhardness value for pristine tungsten specimen is nearly 722 ± 17 MPa, and after gold ion irradiation microhardness has increased to a value of 777 ± 10 MPa. The increase in microhardness of irradiated tungsten indicates the increase in resistance to plastic deformation for irradiated tungsten. The increase in resistance to plastic deformation owes its origin in increased number of defects. The plastic flow in irradiated tungsten specimen is getting inhibited by defects as lattice imperfections anchor dislocation movements.

During the passage of energetic gold heavy ions through the tungsten lattice, displacement and ionization of tungsten atoms take place. The tungsten atom and electrons of the tungsten atom both absorb energy from the fast moving ions and it is believed that nuclear and electronic losses, both are contributing in damage creation in present case, however regime is different. It is evidenced from TRIM calculations that 84% of incident energy of each ion (120 MeV gold ions) is transferred for ionization of tungsten atoms. Therefore, it is anticipated that energy imparted to the electronic system via inelastic electronic losses is getting transferred to the atomic system by electron-phonon coupling, which subsequently leads for defect creation in tungsten lattice. This can be understood by invoking inelastic thermal spike model, which was proposed for metals [46]. According to thermal spike model, kinetic energy of the electrons is transmitted to the atomic system of target atoms by electron-phonon interaction, which results in the increase of local lattice temperature. TRIM calculation reveals that ~ 95274 vacancies per ion get produced when gold ions of energy 120 MeV passes through the tungsten lattice and recoil cascades cause $95274 \times$ lattice binding energy of tungsten ($=3 \text{ eV}$) i.e. 286 KeV phonons. It suggests that in localized spatial region the atoms will have high kinetic energy, and the lattice structure in the region will be driven to highly disordered crystalline state. Thus it is believed that defect generation in tungsten lattice is due to energy transfer from electronic system to atomic system by electron-phonon coupling in addition to nuclear losses. Eventually, sufficient amount of energy is being deposited by gold ions in atomic system for generation of defects in tungsten lattice.

4. Conclusions

By employing energetic heavy ion irradiation, defect centres have successfully been generated in tungsten. Variation of positron lifetime for pristine and irradiated tungsten specimens confirms

evolution of different kind defect centre under energetic heavy ion irradiation. X-ray diffraction result suggests introduction of tensile inhomogeneous micro strain in tungsten lattice on heavy ion irradiation. There is no evidence of major structural phase transformation in irradiated tungsten specimen. However, interestingly XRD of PW:1.5e14 tungsten specimen (having substantial amount of compressive micro-strain before irradiation) indicates grain growth and on other hand XRD of AW:1.5e14 tungsten specimen (having no micro-strain before irradiation) indicates grain refinement. Both the measurements, electrical and microhardness on pristine and irradiated tungsten specimen indicate the generation of defects inside tungsten as well. The defect generation in tungsten is explained with help of inelastic thermal spike model. The energetic heavy ions deposit most of their energy in electronic system. The energy transfer from electronic to atomic system contributes extensively in atomic arrangements, which is responsible for defect creation inside tungsten specimen. However, further investigations need to be carried to understand the intriguing physics behind the damage creation and grain growth/refinement.

Acknowledgement

Help from Pelletron group at IUAC is highly acknowledged. Authors extend their gratitude to TBM division, Institute for Plasma Research, Gandhinagar for extending microhardness facility for mechanical characterization of specimens. Authors are thankful to Dr. S. C. Kashyap, Thin Film Laboratory, Department of Physics, Indian Institute of Technology Delhi for providing their facility for electrical characterization of pristine and irradiated tungsten specimen.

References

- [1] M.R. Gilbert, S.L. Dudarev, S. Zheng, L.W. Packer, J. Ch Sublet, Nucl. Fusion 52 (2012) 083019.
- [2] D. Stork, P. Agostini, J.-L. Boutard, D. Buckthorpe, E. Diegele, S.L. Dudarev, C. English, G. Federici, M.R. Gilbert, S. Gonzalez, A. Ibarra, C. Linsmeier, A.L. Puma, G. Marbach, L.W. Packer, B. Raj, M. Rieth, M.Q. Tran, D.J. Ward, S.J. Zinkle, Fusion Engg. Des. 89 (7–8) (2014) 1586.
- [3] G. Pintsuk, I. Uytendhouwen, Int. J. Ref. Met. Hard Mater. 28 (2010) 661.
- [4] V. Barabash, G. Federici, M. Rodig, L.L. Snead, C.H. Wu, J. Nucl. Mater. 283–287 (2000) 138.
- [5] J. Roth, E. Tsitrone, A. Loarte, Th Loarer, G. Counsell, R. Neu, V. Philipps, S. Brezinsek, M. Lehnen, P. Coad, Ch Grisolia, K. Schmid, K. Krieger, A. Kallenbach, B. Lipschultz, R. Doerner, R. Causey, V. Alimov, W. Shu, O. Ogorodnikova, A. Kirschner, G. Federici, A. Kukushkin, J. Nucl. Mater. 390–391 (2009) 1.
- [6] D.E.J. Armstrong, A.J. Wilkinson, S.G. Roberts, Phys. Scr. T145 (2011) 014076.
- [7] C.D. Hardie, C.A. Williams, S. Xu, S.G. Roberts, J. Nucl. Mater. 439 (2013) 33.
- [8] D. Kanjilal, Curr. Sci. 80 (12) (2001) 1560.
- [9] L. Thome, A. Debelle, F. Garrido, S. Mylonas, B. Decamps, C. Bachelet, G. Sattonnay, S. Moll, S. Pellegrino, S. Miro, P. Trocellier, Y. Serruys, G. Velisa, C. Grygiel, I. Monnet, M. Toulemonde, P. Simon, J. Jagielski, I.J. Biala, L. Nowicki, M. Behar, W.J. Weber, Y. Zhang, M. Backman, K. Nordlund, F. Djurabekova, Nucl. Instru. Meth. Phys. Res. B 307 (2013) 43.
- [10] Y. Oya, M. Shimada, M. Kobayashi, T. Oda, M. Hara, H. Watanabe, Y. Hatano, P. Calderoni, K. Okuno, Phys. Scr. T145 (2011) 014050.
- [11] M.A. Kirk, M. Li, P. Baldo, Microsc. Microanal. 15 (S2) (2009) 1348.
- [12] J. Gibson, D. Armstrong, S. Roberts, Phys. Scr. T159 (2014) 014056.
- [13] I. Takagi, K. Yamamichi, Y. Furuta, M. Akiyoshi, H. Tsuchida, Y. Hatano, T. Sasaki, J. Nucl. Mater. 442 (2013) S246.
- [14] M. Shimada, G. Cao, Y. Hatano, T. Oda, Y. Oya, M. Hara, P. Calderoni, Phys. Scr. T145 (2011) 014051.
- [15] M. Shimada, G. Cao, T. Otsuka, M. Hara, M. Kobayashi, Y. Oya, Y. Hatano, Nucl. Fusion 55 (2015) 013008.
- [16] M. Shimada, Y. Hatano, P. Calderoni, T. Oda, Y. Oya, M. Sokolov, K. Zhang, G. Cao, R. Kolasinski, J.P. Sharpe, J. Nucl. Mater. 415 (2011) S667.
- [17] Y. Hatano, M. Shimada, T. Otsuka, Y. Oya, V. Kh Alimov, M. Hara, J. Shi, M. Kobayashi, T. Oda, G. Cao, K. Okuno, T. Tanaka, K. Sugiyama, J. Roth, B. Tyburska-Puschel, J. Dorner, N. Yoshida, N. Futagami, H. Watanabe, M. Hatakeyama, H. Kurishita, M. Sokolov, Y. Katoh, Nucl. Fusion 53 (2013) 073006.
- [18] B.I. Khripunov, V.M. Gureev, V.S. Koidan, S.N. Kornienko, S.T. Latushkin, A.I. Ryazanov, E.V. Semenov, V.G. Stolyarova, L.S. Danelyan, V.S. Kulikauskas, V.V. Zatekin, V.N. Unezhev, V.B. Petrov, J. Nucl. Mater. 438 (2013) S1014.
- [19] O.V. Ogorodnikova, Y. Gasparyan, V. Efimov, L. Ciupinski, J. Grzonka, J. Nucl. Mater. 451 (2014) 379.
- [20] O.V. Ogorodnikova, K. Sugiyama, J. Nucl. Mater. 442 (2013) 518.
- [21] L. Ciupinski, O.V. Ogorodnikova, T. Plocinski, M. Andrzejczuk, M. Rasinski, M. Mayer, K.J. Kuzydlowski, Nucl. Instr. Meth. Phys. Res. B B317 (2013) 159.
- [22] Z.G. Wang, Ch Dufour, E. Paumier, M. Toulemond, J. Phys. Condens. Mater. 6 (1994) 6733.
- [23] M. Toulemonde, C. Dufour, E. Paumier, Acta Phys. Pol. A 109 (2006) 311.
- [24] S.L. Daraszewicz, Y. Giret, H. Tanimura, D.M. Duffy, A.L. Shluger, K. Tanimura, Appl. Phys. Lett. 105 (2014) 023112.
- [25] Z.G. Wang, Ch Dufour, E. Paumier, M. Toulemonde, J. Phys. : Condens. Mater. 6 (1994) 6733.
- [26] G.K. Mehta, Nucl. Instru. Meth. Phys. Res. A 382 (1996) 335.
- [27] A. Gupta, D.K. Awasthi, Phys. Rev. B 64 (2001) 155407.
- [28] J. F. Ziegler, J. P. Biersack, U. Littmark, The Stopping and Range of Ions in Solids. New York: Pergamon Press.
- [29] P. Kikegaard, M. Eldrup, O.E. Mogensen, N.J. Pedersen, Comp. Phys. Comm. 23 (3) (1981) 307.
- [30] Z. Shengyun, X. Yongjun, W. Zhiqiang, Z. Yongnan, Z. Dongmei, D. Enpeng, Y. Daqing, M. Fukuda, M. Mihara, K. Matsuta, T. Minamisono, J. Nucl. Mater. 343 (2005) 330.
- [31] P.E. Lhuillier, M.F. Barthe, P. Desgardin, W. Egger, P. Sperr, Phys. Status Solidi C 6 (11) (2009) 2329. M. J. Puska, M. Sob, G. Brauer, T. Korhonen, J. Phys. IV 5 (1995) 135; R. Ziegler, H. E. Schaefer, Mater. Sci. Forum. 15 (1987) 145; P. M. G. Nambissan, P. Sen, Rad. Eff. 124 (1992) 215.
- [32] T. Troev, E. Popov, N. Nankov, T. Yoshiie, J. Phys. Conf. Ser. 207 (2010) 012033.
- [33] A. Debelle, M.F. Barthe, T. Sauvage, J. Nucl. Mater. 376 (2008) 216–221.
- [34] Y. Yamamoto, J. Yoshimatsu, K. Morishit, J. Nucl. Mater. 442 (2013) S773.
- [35] B.A. Loomis, S.B. Gerber, J. Nucl. Mater. 117 (1983) 224.
- [36] J.L. Brimhall, E.P. Simonen, L.A. Charlot, J. Nucl. Mater. 117 (1983) 118.
- [37] S. Kumari, D.K. Snigh, P.K. Giri, J. Nanosci. Nanotech. 9 (2009) 1.
- [38] R.M. German, Crit. Rev. Solid State Mater. Sci. 35 (2010) 263.
- [39] G.S. Was, Fundamentals of Radiation Materials Science: Metals and Alloys, 2007 ed., Springer, 2007.
- [40] H. Wang, Y. Gao, E. Fu, T. Yang, S. Yan, J. Xue, Y. Wang, P.K. Chu, J. Nucl. Mater. 442 (2013) 189.
- [41] G.S. Was, J.W. Jones, C.E. Kalnas, L.J. Parfitt, M. Goldiner, Surf. Coat. Tech. 65 (1994) 77.
- [42] M. Fukuda, A. Hasegawa, T. Tanno, S. Nogami, H. Kurishita, J. Nucl. Mater. 442 (2013) S273.
- [43] A. Dunlop, D. Lesueur, G. Jaskierowicz, J. Schildknecht, Nucl. Instr. Meth. Phys. Res. B B36 (1989) 412.
- [44] B. Fu, W. Lai, Y. Yuan, H. Xu, W. Liu, J. Nucl. Mater. 427 (2012) 268.
- [45] N. Wakeham, A.F. Bangura, X. Xu, J.F. Mercure, M. Greenblatt, N.E. Hussey, Nat. Commun. 2 (396) (2011) 1.
- [46] Ch Dufour, A. Audouard, F. Beuneu, J. Dural, J.P. Girard, A. Hairie, M. Levalois, E. Paumier, M. Toulemonde, J. Phys. Condens. Matter. 5 (1993) 4573.